scientific reports

Check for updates

OPEN

Antimicrobial properties of Graphene sheets embedded with Titanium Oxide and Calcium Oxide nanoparticles for industrial wastewater treatment

Reza Darini[1], Hamed Ahari[2]✉, Amir Khosrojerdi[1], Behrooz Jannat[3] & Hossein Babazadeh[1]

This study investigated the antimicrobial efficacy of graphene, titanium dioxide nanoparticles (TiO2NPs), and calcium oxide nanoparticles (CaONPs) against various microorganisms in dairy wastewater. The minimum inhibitory concentration (MIC) of graphene was determined to be 41.66 mg/L for Escherichia coli and 33.33 mg/L for Staphylococcus aureus, outperforming TiO2NPs and CaONPs. Additionally, graphene sheets embedded with 2.8% TiO2 (GST2.8) demonstrated superior performance in inhibiting bacterial growth compared to unmodified or other modified graphene sheets. The GST2.8 treatment significantly reduced microbial counts for *S. aureus*, *E. coli*, and mold/yeast, with the lowest observed counts being 4.85 CFU/mL, 3.00 CFU/mL, and 4.04 CFU/mL, respectively. These results suggest that graphene-based nanocomposites incorporating TiO2NPs and CaONPs hold promise as effective antimicrobial agents for wastewater treatment applications.

Keywords Wastewater treatment, Graphene, Graphene-TiO_2, Graphene-CaO, Antimicrobe

Wastewater is a heterogeneous mixture of pollutants that vary in composition depending on their sources. The major pollutants found in wastewater, which can have significant implications for public health, include biodegradable, volatile, and recalcitrant organic compounds, as well as pathogenic microorganisms, like bacteria, viruses, and parasites[1,5]. These contaminants pose a serious threat to human health, as well as the environment, highlighting the need for effective wastewater treatment strategies to mitigate their detrimental effects[2].

The implementation of effective and suitable treatment processes to eliminate pollutants from wastewater is of paramount importance. This not only helps in preserving the environmental and ecological balance but also fosters sustainable industrial development[3]. Recently, the use of nanomaterials has been regarded as a promising strategy for enhancing wastewater treatment due to their unique physicochemical properties. Photocatalysis has recently gained significant attention as an emerging and promising method for wastewater treatment [4,6,7]. Many materials have been suggested as potential photocatalysts, with notable contributions from researchers, such as Kumar, et al.[8], Kumar, et al.[9], and Madani, et al.[10].

The incorporation of nanoparticles (NPs) in wastewater treatment has demonstrated significant potential, with titanium dioxide (TiO_2) and calcium oxide (CaO) standing out due to their distinctive properties and promising outcomes[11,12]. These NPs present significant opportunities to boost the performance of composite materials used in wastewater treatment and sewage sludge processing. Additionally, there has been a significant increase in the use of graphene-oriented materials as well as their derivatives as carriers for NPs in wastewater treatment applications[1]. Today, TiO_2 is widely recognized as a favorable material for water treatment due to its highly beneficial effects on wastewater purification processes[13]. On the other hand, CaONPs have been used to remove lead from wastewater[14].

Graphene (G), a two-dimensional material containing carbon atoms that are arranged in a hexagonal lattice, is an appropriate material for wastewater treatment because of its large surface area, excellent mechanical properties, and chemical stability[8,15]. The active segments of graphene and its chemically reactive surface facilitate

[1]Department of Water Science and Engineering, Science and Research Branch, Islamic Azad University, Tehran, Iran. [2]Department of Food Science and Technology, Science and Research Branch, Islamic Azad University, Tehran, Iran. [3]Food and Drug Administration, Ministry of Health and Medical Education, Tehran, Iran. ✉email: dr.h.ahari@gmail.com

its strong adhesion to both prokaryotic and eukaryotic cells. Graphene has been shown to operate through a physical mechanism, disrupting the bacterial membrane and inflicting damage to the cell wall, which ultimately leads to bacterial death[16]. G-based materials enable the generation of nanocomposites with other materials, as different kinds of nanomaterials are immobilized onto graphene nanosheets. This approach enhances the functionality of both materials and can lead to the development of synergistic properties[17].

Recent studies have highlighted the potential of graphene-based polymeric composites for antimicrobial applications. These materials, characterized by their unique physical and chemical properties, exhibit strong antimicrobial activity against a broad spectrum of microorganisms [18,19]. The sharp edges of graphene-based materials can physically damage bacterial cell membranes, leading to cell death. Additionally, the large surface area of graphene allows for efficient adsorption of bacterial cells, further contributing to their antimicrobial efficacy[20]. By incorporating graphene-based materials into polymeric composites, researchers have developed innovative materials with enhanced antimicrobial properties, which can be applied in various fields, including medicine, food packaging, and water treatment [21,22].

The antimicrobial mechanism of action of the graphene-based nanocomposites likely involves a combination of factors, including physical disruption of cell membranes, oxidative stress, and pH effects. The sharp edges of graphene sheets can physically damage bacterial cell membranes, leading to cell death. Additionally, the large surface area of graphene allows for efficient adsorption of bacterial cells. The incorporation of TiO2 and CaO nanoparticles further enhances the antimicrobial properties of the composites. TiO2 nanoparticles can generate reactive oxygen species (ROS) upon exposure to light, which can damage cellular components and lead to cell death[23]. CaO nanoparticles can alter the pH of the surrounding environment, creating conditions that are unfavorable for bacterial growth. The synergistic effect of these mechanisms contributes to the observed antimicrobial activity of the graphene-based nanocomposites[24].

The incorporation of graphene into nanocomposites enhances adsorption capabilities, generates catalytically active sites, and improves electron transfer and separation from the TiO_2 conduction band[25]. The combination of TiO_2 with partially reduced graphene oxide (rGO) can enhance the photocatalytic activity by an increase in the adsorption capacity of reactants and a decrease in the recombination of charge carriers, among other advantages[26]. However, the use of G in wastewater treatment is still facing some challenges, such as the aggregation of graphene sheets (GSs), which can reduce its adsorption capacity and surface area[27]. To overcome these challenges, researchers have focused on modifying GSs with NPs to enhance their properties and performance in wastewater treatment[28].

Generally, TiO_2NPs are known for their photocatalytic activity. This activity allows them to produce reactive oxygen species (ROS) when exposed to light, which in turn leads to the degradation of organic pollutants, and the reduction of antibiotic[29] or microbial loads[27,30]. On the other hand, CaONPs can alter the pH of wastewater and cause damage to the cell membrane of microorganisms, resulting in their death[31]. We aimed to assess the efficacy of modified GSs embedded with TiO_2NPs and CaONPs in reducing the microbial loads of diverse microorganisms in wastewater (WW) samples. We synthesized a variety of modified GS samples and evaluated their performance in comparison to unmodified GS and control WW samples.

Materials and methods

Materials and chemicals

Natural graphite powder (purity, 98.0%), TiO_2, CaO, potassium permanganate ($KMnO_4$; purity, 99.0%), hydrochloric acid (HCl, 38.0%), sulfuric acid (H_2SO_4, 95.0%), hydrogen peroxide (H_2O_2; 30.0%), and a peptone solution were purchased from Merck (Germany). The Mueller-Hinton broth, Mueller-Hinton agar (MHA), De Man, Rogosa, and Sharpe (MRS) agar, and nutrient agar culture medium, which were used to cultivate targeted bacteria, were also prepared by Sigma-Aldrich (MO, USA). In all experiments, deionized (DI) water, purified in a Milli-Q® system (Merck Millipore, Germany), was used. All chemical agents were of an analytical grade.

Synthesis of graphene

Graphene was produced by a modified version of the well-established Hummers' approach[32]. Initially, graphite powder (0.5 g) was mixed with 25 mL of concentrated sulfuric acid at 50–60 °C for 30 min. The mixture was subjected to sonication for an hour, which helped to reduce the temperature to approximately 4–5 °C, by an ice bath. During this process, potassium permanganate (3 g) was gradually added and mixed by stirring, followed by adding 0.5 g of sodium nitrate to the mixture, serving as a catalyst[33]. The carbon atoms in graphite then underwent to be oxidized by potassium permanganate, leading to the generation of graphene. This mixture was then stirred for two hours at room temperature[34]. Next, deionized water (100 mL) and H_2O_2 (5 mL) were added to the mixture to remove any remaining oxidizing agents and reduce graphene oxide (GO) to graphene[35]. Next, graphene was centrifuged and washed using deionized water until it reached a neutral pH. It was then reduced to graphite using a reducing agent, such as hydrazine[36].

Synthesis of G-TiO2NPs (or CaONPs)

For the synthesis of graphene-TiO2 (or CaO) nanocomposites, a specified amount of TiO2 or CaO (Table 1) was dissolved in 4% DMSO using a 150-mL beaker. Subsequently, 0.025 g of graphene and 100 mL of DW were combined in a 280-mL flask and subjected to sonication with a Q700 Sonicator (Qsonica) at 100 Watts and 20 kHz for 30 min to achieve a homogeneous solution. The TiO_2 or CaO solution was then added to the flask, followed by refluxing for eight hours at 80 °C. After centrifuging and washing the mixture with DW, the powder was dried at 60 °C and annealed at 400–500 °C under an argon atmosphere to improve the crystallinity of the nanocomposite[37].

Groups	Graphite	TiO_2-NP	CaO-NP
G	*	–	–
GT1.4%	*	½ MBC	–
GT2.8%	*	MBC	–
GC2.5%	*	–	½ MBC
GC5.0%	*	–	MBC

Table 1. Study design of graphene sheets (GSs) composed of graphite embedded with TiO_2NPs or CaONPs. *MBC* minimum bactericidal concentration.

Characterization of G-TiO2NPs (or CaONPs)

The G-TiO_2NPs (or CaONPs) were characterized by X-ray diffraction (XRD) analysis. The XRD patterns related to the fabricated films were acquired using CuKα radiation, operating at a voltage of 40 kV and a current of 45 mA[38]. The patterns were recorded over a range of 5–80° for the 2θ angle, which is the angle between the detector and the incident X-ray beam. The obtained XRD patterns were analyzed to determine the crystal structure and phase composition of G-TiO_2NPs (or CaONPs). The G-TiO_2NPs (or CaONPs) were characterized using the Fourier-transform infrared spectroscopy (FTIR). The FTIR spectra of the specimens were achieved by the attenuated total reflectance (ATR) technique, as part of the smart FTIR method[38]. For each spectrum, 64 consecutive scans were acquired by the spectrometer from 400 to 4000 cm^{-1}, with a precision of 1–4 cm^{-1}.

An ion chromatography (IC) analysis was performed on the sample before and after it was processed through ion exchange resins, using a conductive detector for 24 min at an injection pressure of 4.9 MPa and a flow rate of 9.3 mL/min, in accordance with the instrument's instructions. Cationic and anionic chromatograms were generated using the MagIC Net software. The G-TiO_2 (or CaO) nanocomposite was characterized via scanning electron microscopy (SEM; Cambridge S 360, UK). Generally, SEM is a powerful imaging technique that allows for investigating the morphology and structure of nanocomposites at a nanoscale. The samples were prepared by cutting them into dimensions of 8 × 8 mm and a thickness of 3 mm. They were then mounted onto an SEM stub and coated with a conductive layer of gold for analysis. The SEM setting was adjusted to obtain clear images of the nanostructure. The imaging software was utilized to analyze the results, enabling the measurement of particle dimensions and the examination of their morphology[37].

Evaluation of antibacterial activity (phase 1)

In the first phase of the antibacterial evaluation, the MHA culture medium was prepared by dissolving MHA powder (14 g) in 1 L of DW. The solution was then sterilized in an autoclave. Following sterilization, the medium was poured into sterile plates and allowed to set for up to 15 min. A bacterial suspension was provided to match the 0.5 McFarland turbidity standard (1.5 × 10^8 colony-forming units per milliliter (CFU/mL)), using isolated colonies of E. coli (ATCC 25922) and S. aureus (ATCC 25923). These colonies were obtained from the Institute of Standards and Industrial Research of Iran (ISIRI) and are recognized with the code l124 in the Persian Type Culture Collection (PTCC)[39]. A sterile swab was used to spread the bacterial suspension on the surface of the MHA medium. Antibiotic disks (methicillin, vancomycin, amoxicillin, erythromycin, streptomycin, tetracycline, and cefixime) were placed on the plate surface, and the plates underwent incubation at 37 °C for 24 h. Following 24 h, the growth inhibition halo diameter was measured.

For the assessment of minimum inhibitory concentration (MIC) values of graphene, graphene nanocomposite-TiO2NPs, and CaONPs, varying concentrations of these compounds were introduced into a microbial broth culture. The broth cultures were prepared using Mueller-Hinton broth, and the bacterial suspensions were adjusted to the 0.5 McFarland standard. These cultures were then incubated at 37 °C for 24 h. The lowest concentration of the compounds that inhibited bacterial growth was regarded as the MIC.

Bacterial evaluation of effluents (phase 2)

In the following stage of the antibacterial evaluation, wastewater obtained from the equipment washing section of a dairy factory was systematically passed through individual GSs. The plates were positioned on a Büchner funnel, and a defined volume of wastewater was directed through each plate. The microbial assessment encompassed the comparison of the primary effluent sample with the effluents that traversed each GS. The assessment parameters included the total microbial load, the presence of mold or yeast, as well as the detection of *E. coli* and *S. aureus*. Each sample was subjected to a series of dilutions using a 0.1% peptone solution. Subsequently, either 1 mL or 0.1 mL of each dilution was utilized appropriately. The total microbial count was quantified by performing three repetitions of either pour-plate or surface culture techniques on selective agar plates[40].

Viable mesophilic bacteria were quantified using the Plate Count Agar (PCA) culture medium, followed by incubation at 30 °C for 48 h. The total CFU per milliliter (CFU/mL) was determined using the Violet Red Bile Glucose (VRBG) agar culture medium. Enumeration was carried out on plates that contained 30 to 300 colonies. The enumeration of *Salmonella* was conducted in accordance with the procedures specified in the Iranian Standard No. 1810. Meanwhile, the Baird-Parker agar culture medium was employed to detect the presence of *S. aureus*[39]. Also, the enumeration of mold and yeast was carried out using the Yeast Dextrose Carbonate (YDC) agar culture medium, which was incubated at 25 °C for 3–5 days. Finally, the presence of *E. coli* was determined by the Most Probable Number (MPN) approach[39].

	E. coli	S. aureus
Graphene	41.66 ± 0.05^{aA}	33.33 ± 0.05^{aB}
TiO_2NP	16.66 ± 0.07^{bA}	8.33 ± 0.07^{bB}
CaONP	20.83 ± 0.07^{bA}	16.66 ± 0.07^{bB}

Table 2. Minimum inhibitory concentrations (MIC, mg/L) of graphene, TiO_2NP, and CaONPs against *Staphylococcus aureus* and *Escherichia coli*.

	E. coli	S. aureus
Graphene	7.33 ± 0.05^{bA}	7.66 ± 0.03^{bA}
TiO_2NP	9.66 ± 0.07^{aA}	10.33 ± 0.04^{aA}
CaONP	7.66 ± 0.07^{bA}	8.66 ± 0.04^{bA}

Table 3. Comparison of the inhibition zone diameter (mm) in different treatments against targeted bacteria.

Statistical analysis

Data are reported as mean ± standard error (SE). One-way analysis of variance (ANOVA) compared the data obtained from the experiments. In cases where the overall effect of treatment was found to be statistically significant, a post-hoc analysis using Duncan's multiple range test determined differences between the mean values. For comparisons between two groups, the two-sample t-test was utilized. Data analyses were conducted in SPSS 26, and a significance level of $P \leq 0.05$ was established for all data comparisons[41].

Results and discussion

Table 2 compares the mean MICs of graphene, TiO_2NPs, and CaONPs against two targeted bacteria, namely *S. aureus* and *E. coli*. Graphene had the highest MIC ($P \leq 0.05$) against both bacteria, with values of 41.66 and 33.33 mg/L for *E. coli* and *S. aureus*, respectively, whereas no significant difference was found in the MICs of TiO_2NPs (16.66 and 8.33 mg/L, respectively) and CaONPs (20.83 and 16.66 mg/L, respectively) against these bacteria ($P > 0.05$). However, the MIC against *S. aureus* was found to be significantly lower than that against *E. coli* in all three groups tested ($P \leq 0.05$). This observation could be due to the higher effectiveness of both TiO_2/CaONPs and graphene against Gram-positive bacteria, like *S. aureus*, compared to Gram-negative bacteria. Similarly, the concentration of CaO powder that completely inhibited the growth rate was 5.08 mg/L for *S. aureus* and 3.06 mg/L for *E. coli*[42].

The MICs of CaONPs (25%) loaded with polylactic acid (0.5%) against *E. coli* and *S. aureus* were respectively 2 and 4 µg/L[43]. Similarly, the MIC for both bacteria was determined to be 3.9 µL/mL of CaO[44]. Contrarily, another study reported MIC values of 1.5 and 2 mg/mL for *E. coli* and *S. aureus*, respectively[45]. These disparities in the MIC values among the aforementioned studies could be because of differences in the composition, size, concentration, and surface features of NPs, as well as differences in bacterial strains and even experimental conditions used in each study[45].

A study conducted on graphene[46] reported MIC values against *S. aureus* and *E. coli* of 0.06 and 0.50 mg/L, respectively, which are significantly lower than the results of our study (Table 2). The higher MIC values of G compared to TiO2NPs and CaONPs could be attributed to the different mechanisms of action of the materials or the type of bacteria. Gram-positive bacteria were more susceptible to NPs than Gram-negative bacteria, probably because of differences in their cell wall structure. It should be noted that Gram-positive bacteria with a thick peptidoglycan layer in their cell wall are more vulnerable to the antimicrobial effects of metal NPs [48,49]. On the other hand, TiO2NPs have been shown to have a chemical mechanism of action, where they generate ROS responsible for oxidative stress and damage to bacterial DNA, proteins, and lipids[50].

The results of our study showed that the bacterial communities in biofilms formed on different pipe materials were highly similar, as indicated by both alpha and beta diversity analyses. This suggests that the pipe material may not significantly shape the composition and diversity of bacterial communities in the biofilm. These findings contradict some previous studies that have reported differences in bacterial communities based on pipe material ,[52,53]. However, the results or data that support any conclusions shown directly or otherwise publicly available according to the standards of the field. This discrepancy could be due to variations in experimental conditions, bacterial strains, or analytical methods used in different studies.

Lowercase letters (a & b) in each column denote significant differences between different materials tested ($P \leq 0.05$). Uppercase letters (A & B) show significant differences in the MIC values between the two bacterial strains for each material tested ($P \leq 0.05$).

Table 3 presents a comparative analysis of the inhibition zone diameters among different groups against two target bacteria, *Staphylococcus aureus* and *Escherichia coli*. The mean inhibition zone diameter for *E. coli* was highest in the TiO2NP group (9.66 mm), followed by the CaONP group (7.66 mm), and the unmodified graphene group (7.33 mm). Similarly, Vi, et al.[54] reported antibacterial activities of graphene against *E. coli* and *S. aureus* with inhibition zones of 9.5 mm and 9.0 mm, respectively. These results contrast with those of Aunkor, et al.[55], who observed significantly larger inhibition zones (39 mm and 38 mm, respectively) for the same bacterial

strains. The discrepancies in these measurements may be attributed to differences in the composition of the compounds tested, particularly the urine samples obtained from patients.

In a study by Hashemi et al. (2019), graphene nanoparticles (GNPs) were synthesized and their antibacterial effects on *Staphylococcus aureus* and *Escherichia coli* were evaluated[56]. The study reported that both reduced graphene oxide (rGO) and GNPs exhibited toxicity towards the bacteria, with bacterial growth reduction observed at concentrations of 10 and 100 µg/mL. Additionally, Hegyi, et al.[57] compared the effects of TiO2 nanoparticles (TiO2NPs) and TiO2 on *S. aureus* and *E. coli*. They found that the inhibition zone diameters for *E. coli* exposed to 1.0% TiO2NPs and TiO2 were 32.0 mm and 31.5 mm, respectively. For *S. aureus*, the inhibition zone diameters were 20.0 mm and 29.0 mm, respectively, at the same concentration of TiO2NPs and TiO2. These results indicate larger inhibition zones compared to our study (Table 3). In our study, the mean inhibition zone diameter for *S. aureus* was highest in the TiO2NP group (10.33 mm), followed by the CaONP group (8.66 mm) and the unmodified graphene group (7.66 mm).

The CaO/low-density polyethylene (LDPE) nanocomposites containing 25 nm CaO particles showed a reduction in *E. coli* bacteria, ranging from 12 to 30%, depending on the weight of the samples[58]. When exposed to 25 µL of CaO, the inhibition zones for *E. coli* and *S. aureus* were measured to be respectively 24.0 and 22.0 mm. In another study, it was discovered that the MIC for both types of bacteria was 3.9 µL/mL when exposed to CaO[44]. A significant difference was detected in the mean inhibition zone diameter between the groups for both *S. aureus* and *E. coli*. Specifically, the average inhibition zone diameter for the group treated with TiO_2NPs was significantly larger than that of the G and CaONP groups. This observation was consistent for both *S. aureus* and *E. coli* bacteria ($P \leq 0.05$). However, no significant difference was found in the mean inhibition zone diameter between the G and CaONP groups for either *E. coli* or *S. aureus* ($P > 0.05$).

Lowercase letters (a & b) are used to show significant differences between different materials in each column ($P \leq 0.05$). Uppercase letters (A & B) show significant differences in the MIC values between the two bacteria for each material tested ($P \leq 0.05$).

Table 4 presents a comparison of the inhibition zone diameters for different embedded GS samples against two targeted bacteria, *E. coli*, and *S. aureus*, based on the results of the disc diffusion method. There were significant differences in the mean inhibition zone diameter between the groups for both *S. aureus* and *E. coli* ($P \leq 0.05$). Sand functionalized with graphene showed a distinct inhibition zone diameter of 20 mm against *E. coli*. The adsorption experiments demonstrated that the graphene-sand composite efficiently removed contaminants at a concentration of 0.2 g[59]. Following a 10-minute incubation period, the bactericidal effect of G on *E. coli* was twice as potent as its effect on *S. aureus* and five times more potent than its effect on *Streptococcus mutans*[60]. This observation is markedly different from the results of the current study, which found no significant difference in susceptibility between *E. coli* and *S. aureus* (Table 4).

Notably, Gram-positive bacteria demonstrated greater susceptibility to graphene sheets (GS) compared to Gram-negative bacteria[61]. Current literature reveals a significant gap in studies focusing on the incorporation of calcium oxide (CaO) into graphene. The GS + 2.8% TiO2 (GT2.8) group exhibited the most potent antibacterial effect against both *Escherichia coli* and *Staphylococcus aureus*, with mean inhibition zone diameters of 10.33 mm and 12.00 mm, respectively. These measurements were significantly larger than those observed for all other groups in the study ($P \leq 0.05$). The antibacterial activity of the GS + 1.4% TiO2 (GT1.4) group was also significantly higher than that of the GS group for both *E. coli* and *S. aureus* ($P \leq 0.05$). Similarly, the GS + 5.0% CaO (GC5.0) group demonstrated significantly higher antibacterial activity compared to the GS group for both *S. aureus* and *E. coli* ($P \leq 0.05$).

There was no significant difference in the mean inhibition zone diameter between the GS and GS + 2.5% CaO (GC2.5) groups for either *E. coli* or *S. aureus* ($P > 0.05$). The GS embedded with 25 g of chlorophenyl exhibited an inhibition zone diameter of 11 mm against *E. coli* when the bacterial concentration was 30×10^8 CFU/mL[62,63]. However, in this study, a bacterial concentration (1.5×10^8 CFU/mL) resulted in an inhibition zone diameter of 10.33 mm when using GS incorporated with 2.8% TiO_2. Also, the GS embedded with COOH exhibited inhibition zone diameters of 3 mm and 4 mm for *E. coli* and *S. aureus*, respectively[64].

Figure 1 presents the FTIR spectra for five distinct GSs, which were produced using varying concentrations of TiO_2NPs or CaONPs. The spectra provide detailed insights into the chemical bonding and functional groups present in each specimen. The FTIR spectra for all five samples displayed a broad peak from 3400 to 3500 cm^{-1}. This peak was related to the O-H stretching vibrations of C–OH groups and surface hydroxyl from adsorbed water[65]. It also indicated the existence of surface functional groups, like the hydroxyl group, on the GSs. The existence of oxygen-containing groups, like hydroxyl and carboxyl, confirms the oxidation process of graphene

	E. coli	S. aureus
GS	7.66 ± 0.57^{cA}	8.00 ± 0.57^{cA}
GS + 1.4% TiO_2 (GT1.4)	9.33 ± 0.18^{bA}	10.66 ± 0.03^{bA}
GS + 2.8% TiO_2 (GT2.8)	10.33 ± 0.32^{abA}	12.00 ± 0.23^{aB}
GS + 2.5% CaO (GC2.5)	7.33 ± 1.0^{cA}	8.66 ± 0.43^{cA}
GS + 5.0% CaO (GC5.0)	9.00 ± 0.57^{bA}	10.33 ± 0.57^{bA}

Table 4. Inhibition zone diameters (mm) of different embedded graphene sheets (GSs) against targeted bacteria using the disc diffusion method. Lowercase letters (A & B) are used to show significant differences between different materials in each column ($P \leq 0.05$). Uppercase letters (A & B) show significant differences in the MIC values between the two bacteria for each material tested ($P \leq 0.05$). GS: Graphene sheet.

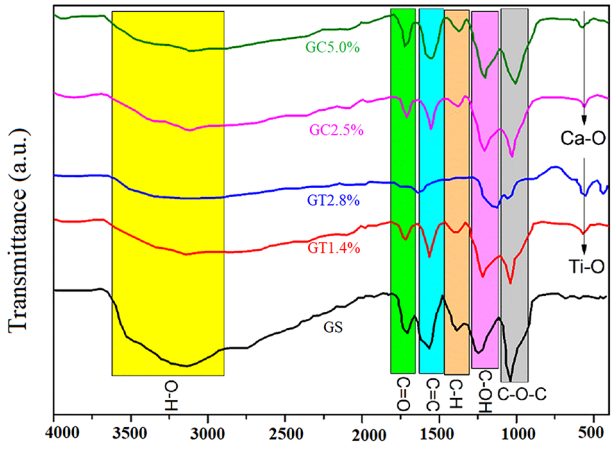

Fig. 1. The FTIR spectra of specimens, including (1) graphene sheets (GSs) composed of graphite (G), (2) GS composed of graphite embedded with 1.4% TiO_2-NP (GT1.4), (3) GS composed of graphite embedded with 2.8% TiO_2-NP (GT2.8), (4) GS composed of graphite embedded with 2.5% CaO-NP (GC2.5), and (5) GS composed of graphite embedded with 5.0% CaO-NP (GC5.0).

in this study[54]. The FTIR spectra also exhibited strong peaks for C=C and C=O (carbonyl stretching) from 1600 to 1700 cm^{-1}. Additionally, the C–OH stretching was found at 1224 cm^{-1}. These peaks corresponded to the two-dimensional sp^5 carbon network character remaining from the GSs[66].

The FTIR spectra of the modified GSs (samples 2–5) showed additional peaks and changes in the peak intensity compared to the spectrum of the unmodified GS (sample 1). The peak observed at 1200–1300 cm^{-1}, which is typically associated with the C-O carbonyl group stretching vibrations, was more prominent in the spectra of the modified GSs. This suggests an increased presence of oxygen-containing functional groups on the GS, which are believed to contribute to the formation of G-TiO_2/CaO nanocomposites. The peak at 1050 cm^{-1} following modification (GT2.8, Fig. 1) shifted to lower wavelengths, related to the existence of a greater concentration of TiO_2 in the GS. This type of shift to other wavelengths has been previously reported by Wanag, et al.[67]. The FTIR spectrum of the modified GSs containing TiO_2NPs and CaONPs showed a broad band below 1000 cm^{-1}, which was attributed to the Ti–O–Ti or Ca–O–Ca stretching and bending vibrational modes. This observation can be explained by the long length of the metal-oxygen bonds in these samples and the relatively low energy required for these bonds to vibrate[68] (Fig. 1). The aforementioned features could potentially explain the antibacterial activity of G-TiO_2/CaO nanocomposites. The introduction of additional functional groups containing oxygen on the surface of the GSs could be a contributing factor, as observed in the disc diffusion assay results presented in Table 4.

Figure 2 presents the XRD patterns for four different modified groups of G-TiO_2/CaO NPs, as well as the unmodified sample (G). These patterns provide valuable information on the crystalline structure and orientation of the samples. Accordingly, the pristine graphene sample showed a single peak at around $2\theta = 1.7^o$, which could be attributed to the (001) plane of the GS. For the graphene samples that were modified with 0.5 MBC of TiO_2NPs, a small peak at $2\theta = 27.1^o$ was observed, in addition to the (001) peak at around $2\theta = 1.7^o$. This additional peak can be attributed to the (101) plane and is characteristic of graphite modified with TiO_2. This peak was not observed in the unmodified GS[69]. This result agrees with those of previous research[66,67], which demonstrated that the peaks on the GS have a highly ordered and layered structure. The energy barrier was higher for few-layer GSs with nooks for penetrating the bacterial lipid bilayer, compared to monolayer sheets of similar lateral size. Therefore, few-layer GSs may have stronger antimicrobial activity compared to monolayer sheets[70].

Other small peaks at $2\theta = 45.0^o$ (200), $2\theta = 54.6^o$ (105), and $2\theta = 64.0^o$ (204) were observed in the XRD pattern. These peaks corresponded to the reference JCPDS code No. 21-1272 for the anatase phase of TiO_2 with a tetragonal crystal system. In the graphene samples modified with 1.0 MBC of TiO_2NPs, a larger peak (compared to the former group) attributed to the (001) plane was observed at $2\theta = 2.4^o$. There were also larger peaks attributed to the (101) plane at $2\theta = 27.2^o$, which are characteristic of graphite with TiO_2. This peak indicated that GS had a highly ordered and layered structure. Also, in the XRD of GSs modified with TiO_2NPs, additional peaks were observed, including the (200) plane at $2\theta = 44.0^o$, the (105) plane at $2\theta = 54.5^o$, and the (204) plane at $2\theta = 63.8^o$ (Fig. 2)[71]. These peaks corresponded to the reference JCPDS code No: 21-1272 for the anatase phase of TiO_2 with a tetragonal crystal system.

In the graphene samples modified with 0.5 and 1 MBC of CaONPs, the XRD pattern revealed additional small peaks, which could be attributed to the (111) plane at $2\theta = 37.8^o$, the (200) plane at $2\theta = 45.5^o$, and the (220) plane at $2\theta = 53.9^o$. The peaks observed were found to correspond to the cubic phase of CaO, as indicated by the reference JCPDS code No. 77-2376. This result is in line with those of Khine, et al.[72]. The XRD patterns indicated that with an increase in the amount of TiO_2 and CaO from 0.5 to 1 MBC, there was a corresponding increase in the intensity of the crystal peaks[69].

Figure 3 displays the SEM images of five graphene specimens, which were either modified or unmodified with TiO_2 or CaO NPs. The SEM images of the unmodified graphene sample (Fig. 3A) indicated a flatter and

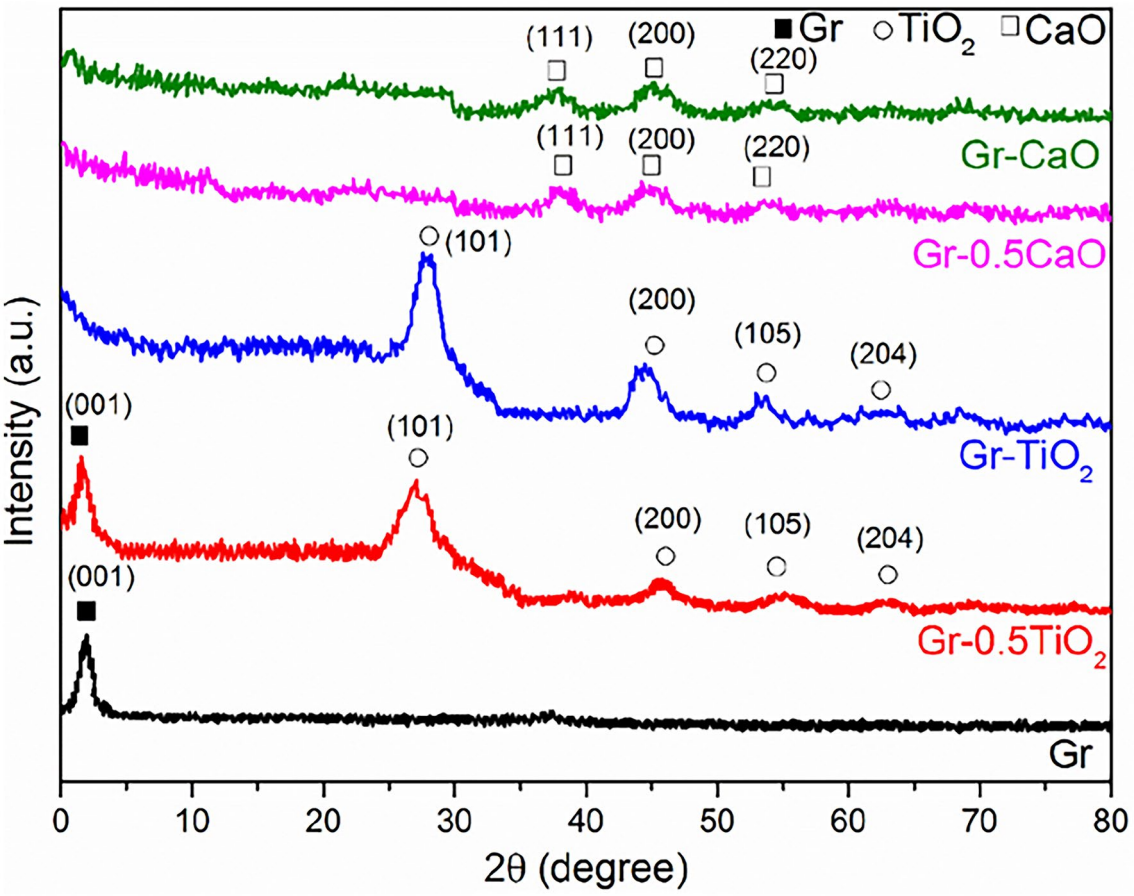

Fig. 2. The X-ray diffraction (XRD) patterns of samples, including (1) graphene, (2) graphene modified with 0.5 MBC of TiO_2NPs, (3) graphene modified with 1 MBC of TiO_2NPs, (4) graphene modified with 0.5 MBC of CaONPs, and (5) graphene modified with 1 MBC of CaONPs.

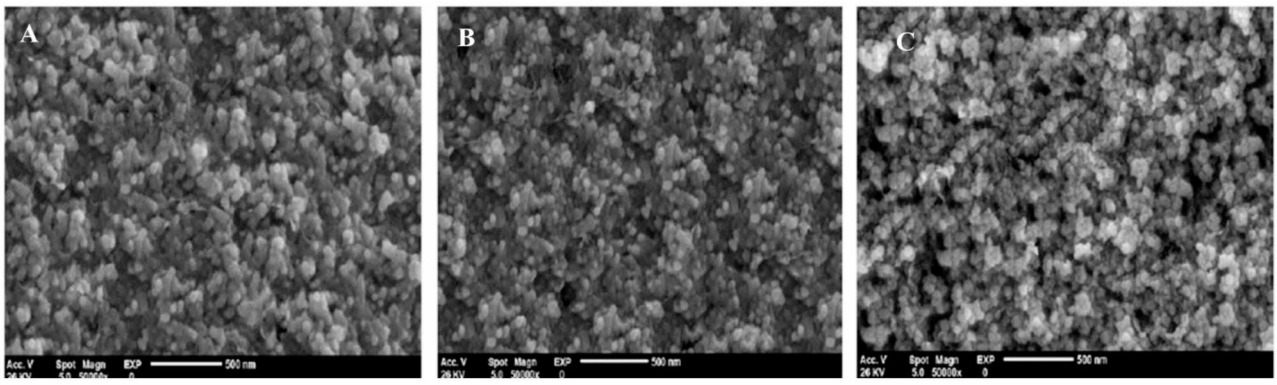

Fig. 3. Scanning electron microscopy (SEM) of samples, including (**A**) graphene sheets (GSs) composed of graphite (G), (**B**) GS composed of graphite with 1.4% TiO_2 (GT1.4), (**C**) GS composed of graphite with 2.8% TiO_2 (GT2.8), (**D**) GS composed of graphite with 2.5% CaO (GC2.5), and (**E**) GS composed of graphite with 5.0% CaO (GC5.0).

smoother surface, with few wrinkles and folds. According to the SEM images of the modified graphene samples (samples B-E), group 3 (Fig. 3C), which consisted of graphene modified with 2.8% TiO_2, exhibited the roughest surface morphology, followed by group 2 (Fig. 3B). These two groups showed a more pronounced surface roughness compared to the other groups (Fig. 3A, D and E). The presence of wrinkles and folds in the GSs

Groups	TBC	Coliform	Salmonella	S. aureus	E. coli	Mold/yeast
WW	8.27 ± 0.00^{a}	5.82 ± 0.00^{a}	3.31 ± 0.00^{a}	6.25 ± 0.00^{a}	3.21 ± 0.00^{a}	4.61 ± 0.00^{a}
GS	7.14 ± 0.01^{b}	5.25 ± 0.01^{b}	3.20 ± 0.01^{a}	6.02 ± 0.01^{b}	3.13 ± 0.01^{b}	4.33 ± 0.01^{b}
GST1.4	6.25 ± 0.01^{e}	4.88 ± 0.01^{c}	2.97 ± 0.01^{b}	5.11 ± 0.01^{c}	3.08 ± 0.01^{b}	4.16 ± 0.01^{c}
GST2.8	6.04 ± 0.02^{f}	4.38 ± 0.02^{d}	2.86 ± 0.02^{b}	4.85 ± 0.02^{d}	3.00 ± 0.02^{c}	4.04 ± 0.02^{d}
GSC2.5	6.89 ± 0.02^{c}	5.16 ± 0.02^{b}	3.07 ± 0.02^{b}	5.67 ± 0.02^{c}	3.16 ± 0.02^{b}	4.25 ± 0.02^{bc}
GSC5.0	6.42 ± 0.07^{d}	4.95 ± 0.07^{b}	3.01 ± 0.07^{b}	5.09 ± 0.07^{c}	3.13 ± 0.07^{b}	4.13 ± 0.07^{c}

Table 5. Microbial loads in dairy wastewater (WW) samples passing through graphene sheets (GSs) modified with CaONPs and TiO_2NPs (log CFU/mL). *WW* Wastewater, *GS* Graphene sheets composed of graphite, *GST1.4* Graphene sheets composed of graphite with 1.4% titanium dioxide, *GST2.8* Graphene sheets composed of graphite with 2.8% titanium dioxide, *GSC2.5* Graphene sheets composed of graphite with 2.5% calcium oxide, *GST5.0* Graphene sheets composed of graphite with 5.0% calcium oxide, *TBC* Total bacterial count. In each column, different letters indicate significant differences ($P \leq 0.05$).

(Fig. 3A) can be attributed to their highly ordered and layered structure, as previously demonstrated by Wang, et al.[73].

The graphene samples modified with TiO_2 or CaO exhibited a more porous and irregular surface, with visible NP agglomerates on the GS surface. This type of structure provides a large surface area of GS that is accessible to NPs. This facilitates the rapid encapsulation of bacteria within the nanopores. In another research by Wanag, et al.[67], the SEM images of *E. coli* cells exposed to TiO_2-GS revealed that the bacterial surface initially adhered smoothly to TiO_2 particles while being partially surrounded by them. However, over time, morphological changes were observed in the bacterial cells. This finding is consistent with our results, as presented in Table 4, which demonstrated a decrease in the number of bacteria, particularly *E. coli* and *S. aureus*, in the GT2.8 group samples. The rougher and more porous surface morphology of the modified graphene samples might have increased the surface area available for interaction with bacteria, leading to increased antibacterial activity. Additionally, the agglomerates of NPs on the surface of the modified graphene samples might have created physical barriers that impeded bacterial growth and colonization.

The unique structural properties of graphene, such as its large surface area and sharp edges, play a crucial role in its antimicrobial activity. The high surface area of graphene enables efficient adsorption of microorganisms, leading to cell death. Additionally, the sharp edges of graphene can physically disrupt the cell membranes of bacteria, causing leakage of cellular contents and ultimately cell lysis. These physical mechanisms, combined with the potential for chemical interactions, contribute to the strong antimicrobial properties of graphene-based materials[74,75].

Table 5 presents the microbial loads in WW samples that were treated with GSs modified with CaONPs and TiO_2NPs. In a previous study, noble metals were uniformly distributed on the TiO_2 and GS surfaces. The TiO_2 photocatalytic activities for degrading two particular pollutants, namely 4-dichlorophenoxyacetic acid and Reactive Red 1952, were investigated in water under both UV and visible light irradiation. Adding noble metals and graphene resulted in a significant enhancement of the photocatalytic activity of TiO_2[76]. This improvement could be attributed to the increased surface area provided by the NPs, which allows for more interaction with pollutants. Additionally, the rate of electron-hole recombination decreased, which promoted a more efficient degradation of pollutants.

The results presented in Table 5 indicate that both the unmodified GS and the wastewater control (WW) exhibited significantly higher microbial loads compared to all modified graphene samples. This observation was consistent across all types of microorganisms tested, including the total bacterial count (TBC), coliform, *Salmonella*, *S. aureus*, *E. coli*, and mold/yeast ($P \leq 0.05$). These findings suggest the role of the nanocomposite G/TiO_2 sheets in reducing microbial populations. When G/TiO_2 nanocomposites are used in water, TiO_2 generates significant amounts of hydroxyl and superoxide radicals through electron transfer. The presence of graphene also contributes to the production of superoxide, which rapidly converts to H_2O_2, ultimately leading to the degradation of organic matter, including bacteria[77].

The findings of a previous study demonstrated the significant antimicrobial effects of the graphene composite material against both *C. albicans* and *S. aureus*, although this effect diminished with higher graphene levels. In contrast, no antimicrobial activity was observed against *E. coli*[78]. The TBC in the unmodified GS was found to be 7.14 log CFU/mL. However, when wastewater was filtered through GS embedded with TiO_2 (GST2.8), there was a significant decrease in the microbial load. The TBC experienced a reduction of 1.1 log across all types of microorganisms. This reduction was significantly greater than that observed in both the unmodified GS sample and the wastewater control.

Notably, the coliform microbial load in GST2.8 demonstrated reductions of 1.44 and 0.87 log CFU/mL compared to the WW samples (Table 5). This indicates that the incorporation of TiO_2NPs, particularly at a concentration of 2.8%, into the GS was highly effective in diminishing the microbial loads. This is likely attributable to the photocatalytic activity of TiO_2. The TiO_2NPs are renowned for their photocatalytic properties, which involve the production of ROS, such as hydroxyl radicals and superoxide radicals when exposed to light. The ROS can react with organic compounds and the cell components of microorganisms. This interaction can cause significant damage to these microorganisms, ultimately leading to their demise[77].

The graphene-TiO2 composite (GST2.8) exhibited significantly lower MIC values (10 and 8 mg/L) compared to graphene alone (41.66 and 33.33 mg/L) for *E. coli* and *S. aureus*, respectively. This indicates a significant improvement in antimicrobial activity, likely due to the synergistic effect of graphene and TiO2 nanoparticles. The enhanced antimicrobial properties of the composite can be attributed to factors such as increased surface area, improved adsorption capacity, and the generation of reactive oxygen species by TiO2 nanoparticles.

Furthermore, the photocatalytic activity of TiO2 may facilitate the degradation of organic pollutants in wastewater, potentially leading to a reduction in microbial load. Among the various modified graphene-based materials evaluated (Table 5), the GST2.8 group demonstrated the lowest bacterial load for *Salmonella*, recorded at 2.86 CFU/mL. Notably, this value did not significantly differ from those observed for other modified graphene-based materials. In this regard, Bykkam, et al.[79] conducted a study involving the use of few-layered GSs embedded with ZnONPs. They reported an inhibition zone diameter of 9 mm for *S. typhi* and 8 mm for *E. coli*. Based on the results presented in Table 5, the GST2.8 group demonstrated the lowest microbial loads for *S. aureus*, *E. coli*, and mold/yeast. Specifically, the enumerated microbial loads for the GST2.8 group were as follows: 4.85 CFU/mL for *S. aureus*, 3.00 CFU/mL for *E. coli*, and 4.04 CFU/mL for mold/yeast.

In another study, in an effort to combat fouling in dairy wastewater treatment and extend the lifespan of the bioreactor membrane, the integration of graphene was explored. This integration proved to be highly effective in removing organic matter, as evidenced by the significant reduction rate of 91.5% for the biochemical oxygen demand and 91.4% for the chemical oxygen demand[80]. Moreover, the antimicrobial properties of a graphene sand composite (GSC) were investigated at two various levels: 0.1 g and 0.2 g. The effectiveness of the GSC was evaluated by measuring the inhibition zone diameter, which represented the area where microbial growth was inhibited. For the 0.1 g concentration of GSC, an inhibition zone diameter of 8 mm was found. Also, a significantly larger inhibition zone (20) mm was observed when the GSC concentration was increased to 0.2 g[59]. This could be potentially attributed to the oxidative stress and membrane stress caused by the sharp wrinkly edges and the nano-layers found in GSC.

In another study, the TiO_2/rGO photocatalytic sheets exhibited an exceptional capability to eliminate *E. coli* from wastewater. Upon exposure to visible-light irradiation, the treatment led to a significant decrease in *E. coli* counts, with an approximate reduction of 8.0 log. In comparison, the treatment conducted without visible-light irradiation resulted in a lower reduction of approximately 1.0 log. These findings highlighted the significant impact of visible-light irradiation on the photocatalytic effect of TiO_2/rGO sheets, leading to enhanced *E. coli* removal from wastewater[81].

In the current study, the presence of CaO/GS composite had an impact on microbial growth and survival rates, as indicated in Table 5. The incorporation of CaONPs into the composite played a potential role in reducing microbial loads by influencing the pH of wastewater[82]. Generally, CaO is characterized as an alkaline substance, and its incorporation into the GS is likely to increase the pH level of the wastewater. This change in pH could potentially affect the growth and survival of microorganisms. Moreover, alkaline conditions have the potential to induce harm to the cell membrane of microorganisms, thereby resulting in cellular death.

While the results of this study demonstrate the promising antimicrobial properties of graphene-based nanocomposites, several practical considerations should be addressed for their large-scale application in wastewater treatment. Scaling up the production of these nanocomposites to industrial levels may pose challenges related to cost-effectiveness and ensuring consistent quality. Furthermore, the long-term stability and potential environmental impacts of these materials in wastewater treatment systems require further investigation.

To address these concerns, future research should focus on developing cost-effective and scalable synthesis methods for graphene-based nanocomposites. Additionally, studies on the environmental fate and toxicity of these materials are crucial to assess their potential risks and ensure their safe and sustainable use.

Conclusion

This study demonstrates the potential of graphene-based nanocomposites for effective microbial control and wastewater treatment. Graphene sheets embedded with titanium dioxide (TiO2) and calcium oxide (CaO) nanoparticles exhibited significant antimicrobial activity against a range of microorganisms, including Escherichia coli, Staphylococcus aureus, and mold/yeast. The modified graphene sheets effectively reduced microbial loads in wastewater samples, particularly for *E. coli* and *S. aureus*. The antibacterial activity is likely attributed to a combination of factors, including physical disruption of bacterial cell membranes, generation of reactive oxygen species, and changes in wastewater pH.

These results highlight the potential of graphene-based nanomaterials as promising candidates for addressing microbial contamination in wastewater treatment processes. However, further research is needed to fully understand the underlying mechanisms, optimize the formulation and application of these materials, and assess their long-term environmental impact. Future studies could focus on evaluating the performance of graphene-based nanocomposites in real-world wastewater treatment plants, investigating their compatibility with other treatment processes, and exploring potential cost-effective production methods.

Data availability

All data generated or analysed during this study are included in this published article.

Received: 2 July 2024; Accepted: 23 December 2024
Published online: 06 January 2025

References

1. Saravanan, A. et al. Effective water/wastewater treatment methodologies for toxic pollutants removal: processes and applications towards sustainable development. *Chemosphere* **280**, 130595 (2021).
2. Naseem, T., Waseem, M., Hafeez, M., Din, S. U. & Haq, S. Reduced graphene oxide/zinc oxide nanocomposite: from synthesis to its application for wastewater purification and antibacterial activity. *J. Inorg. Organomet. Polym Mater.* **30**, 3907–3919. https://doi.org/10.1007/s10904-020-01529-2 (2020).
3. Guieysse, B. & Norvill, Z. N. Sequential chemical–biological processes for the treatment of industrial wastewaters: review of recent progresses and critical assessment. *J. Hazard. Mater.* **267**, 142–152 (2014).
4. Pedanekar, R., Shaikh, S. & Rajpure, K. Thin film photocatalysis for environmental remediation: a status review. *Curr. Appl. Phys.* **20**, 931–952 (2020).
5. Hemdan, B. A., El-Taweel, G. E., Goswami, P., Pant, D. & Sevda, S. The role of biofilm in the development and dissemination of ubiquitous pathogens in drinking water distribution systems: an overview of surveillance, outbreaks, and prevention. *World J. Microbiol. Biotechnol.* **37**, 1–18 (2021).
6. El Nahrawy, A. M., Hemdan, B. A. & Abou Hammad, A. B. Morphological, impedance and terahertz properties of zinc titanate/Fe3 + nanocrystalline for suppression of Pseudomonas aeruginosa biofilm. *Nano-Structures Nano-Objects*. **26**, 100715 (2021).
7. El Nahrawy, A. M. et al. Talented Bi0. 5Na0. 25K0. 25TiO3/oxidized cellulose films for optoelectronic and bioburden of pathogenic microbes. *Carbohydr. Polym.* **291**, 119656 (2022).
8. Kumar, A., Choudhary, P., Kumar, K., Kumar, A. & Krishnan, V. Plasmon induced hot electron generation in two dimensional carbonaceous nanosheets decorated with au nanostars: enhanced photocatalytic activity under visible light. *Mater. Chem. Front.* **5**, 1448–1467 (2021).
9. Kumar, A., Kumar, A. & Krishnan, V. Perovskite oxide based materials for energy and environment-oriented photocatalysis. *ACS Catal.* **10**, 10253–10315 (2020).
10. Madani, S. S. et al. Integration of Bi4O5I2 nanoparticles with ZnO: impressive visible-light-induced systems for elimination of aqueous contaminants. *J. Taiwan Inst. Chem. Eng.* **119**, 177–186 (2021).
11. Palmas, S., Mais, L., Mascia, M. & Vacca, A. Trend in using TiO2 nanotubes as photoelectrodes in PEC processes for wastewater treatment. *Curr. Opin. Electrochem.* **28**, 100699 (2021).
12. Tang, S., Yan, F., Zheng, C. & Zhang, Z. Novel calcium oxide-enhancement phosphorus recycling technique through Sewage Sludge Pyrolysis. *ACS Sustain. Chem. Eng.* **6**, 9167–9177. https://doi.org/10.1021/acssuschemeng.8b01492 (2018).
13. Liu, J. et al. Antimicrobial activity of zinc oxide–graphene quantum dot nanocomposites: enhanced adsorption on bacterial cells by cationic capping polymers. *ACS Sustain. Chem. Eng.* **7**, 16264–16273 (2019).
14. Jalu, R. G., Chamada, T. A. & Kasirajan, R. Calcium oxide nanoparticles synthesis from hen eggshells for removal of lead (pb (II)) from aqueous solution. *Environ. Challenges*. **4**, 100193. https://doi.org/10.1016/j.envc.2021.100193 (2021).
15. Perini, G., Palmieri, V., Ciasca, G., De Spirito, M. & Papi, M. Unravelling the potential of graphene quantum dots in biomedicine and neuroscience. *Int. J. Mol. Sci.* **21**, 3712 (2020).
16. Mohammed, H. et al. Antimicrobial mechanisms and effectiveness of graphene and graphene-functionalized biomaterials. A scope review. *Front. Bioeng. Biotechnol.* **8**, 465 (2020).
17. Lawal, A. T. Graphene-based nano composites and their applications. A review. *Biosens. Bioelectron.* **141**, 111384 (2019).
18. Shi, L. et al. The antibacterial applications of graphene and its derivatives. *Small* **12**, 4165–4184 (2016).
19. Yaragalla, S., Bhavitha, K. B. & Athanassiou, A. A review on graphene based materials and their antimicrobial properties. *Coatings* **11**, 1197 (2021).
20. Díez-Pascual, A. M. & Luceño-Sánchez, J. A. Antibacterial activity of polymer nanocomposites incorporating graphene and its derivatives: a state of art. *Polymers* **13**, 2105 (2021).
21. Fatima, N. et al. Recent developments for antimicrobial applications of graphene-based polymeric composites: a review. *J. Ind. Eng. Chem.* **100**, 40–58 (2021).
22. Avcu, E. et al. Biodegradable polymer matrix composites containing graphene-related materials for antibacterial applications: a critical review. *Acta Biomater.* **151**, 1–44 (2022).
23. Díez-Pascual, A. M. Antibacterial action of nanoparticle loaded nanocomposites based on graphene and its derivatives: a mini-review. *Int. J. Mol. Sci.* **21**, 3563 (2020).
24. Azizi-Lalabadi, M., Hashemi, H., Feng, J. & Jafari, S. M. Carbon nanomaterials against pathogens; the antimicrobial activity of carbon nanotubes, graphene/graphene oxide, fullerenes, and their nanocomposites. *Adv. Colloid Interface Sci.* **284**, 102250 (2020).
25. Thakre, K. G., Barai, D. P. & Bhanvase, B. A. A review of graphene-TiO2 and graphene-ZnO nanocomposite photocatalysts for wastewater treatment. *Water Environ. Res.* **93**, 2414–2460 (2021).
26. Nasr, M. et al. Enhanced visible-light photocatalytic performance of electrospun rGO/TiO2 composite nanofibers. *J. Phys. Chem. C.* **121**, 261–269 (2017).
27. Li, M., Liu, Y., Zeng, G., Liu, N. & Liu, S. -b. Graphene and graphene-based nanocomposites used for antibiotics removal in water treatment: a review. *Chemosphere* **226**, 360–380. https://doi.org/10.1016/j.chemosphere.2019.03.117 (2019).
28. Tabish, T. A., Memon, F. A., Gomez, D. E., Horsell, D. W. & Zhang, S. A facile synthesis of porous graphene for efficient water and wastewater treatment. *Sci. Rep.* **8**, 1817 (2018).
29. Guo, H. et al. Enhanced catalytic performance of graphene-TiO2 nanocomposites for synergetic degradation of fluoroquinolone antibiotic in pulsed discharge plasma system. *Appl. Catal. B.* **248**, 552–566. https://doi.org/10.1016/j.apcatb.2019.01.052 (2019).
30. Dyshlyuk, L. et al. Antimicrobial potential of ZnO, TiO2 and SiO2 nanoparticles in protecting building materials from biodegradation. *Int. Biodeterior. Biodegrad.* **146**, 104821 (2020).
31. Sree, G. V., Nagaraaj, P., Kalanidhi, K., Aswathy, C. & Rajasekaran, P. Calcium oxide a sustainable photocatalyst derived from eggshell for efficient photo-degradation of organic pollutants. *J. Clean. Prod.* **270**, 122294 (2020).
32. Zaaba, N. et al. Synthesis of graphene oxide using modified hummers method: solvent influence. *Procedia Eng.* **184**, 469–477 (2017).
33. Saini, A., Kumar, A., Anand, V. K. & Sood, S. C. Synthesis of graphene oxide using modified Hummer's method and its reduction using hydrazine hydrate. *Int. J. Eng. Trends Technol.* **40**, 67–71 (2016).
34. Paulchamy, B., Arthi, G. & Lignesh, B. A simple approach to stepwise synthesis of graphene oxide nanomaterial. *J. Nanomed. Nanotechnol.* **6**, 1 (2015).
35. Al-Gaashani, R., Najjar, A., Zakaria, Y., Mansour, S. & Atieh, M. XPS and structural studies of high quality graphene oxide and reduced graphene oxide prepared by different chemical oxidation methods. *Ceram. Int.* **45**, 14439–14448 (2019).
36. Guo, Y. et al. One pot preparation of reduced graphene oxide (RGO) or au (ag) nanoparticle-RGO hybrids using chitosan as a reducing and stabilizing agent and their use in methanol electrooxidation. *Carbon* **50**, 2513–2523 (2012).
37. Anirudhan, T. S., Shainy, F. & Christa, J. Synthesis and characterization of polyacrylic acid-grafted-carboxylic graphene/titanium nanotube composite for the effective removal of enrofloxacin from aqueous solutions: Adsorption and photocatalytic degradation studies. *J. Hazard. Mater.* **324**, 117–130 (2017).
38. Adly, M., El-Dafrawy, S. M. & El-Hakam, S. Application of nanostructured graphene oxide/titanium dioxide composites for photocatalytic degradation of rhodamine B and acid green 25 dyes. *J. Mater. Res. Technol.* **8**, 5610–5622 (2019).
39. Asl, N. M., Ahari, H., Moghanjoghi, A. A. M. & Paidari, S. Assessment of nanochitosan packaging containing silver NPs on improving the shelf life of caviar (Acipenser persicus) and evaluation of nanoparticles migration. *J. Food Meas. Charact.* **15**, 5078–5086. https://doi.org/10.1007/s11694-021-01082-7 (2021).

40. Omran, B. & Baek, K. H. Graphene-derived antibacterial nanocomposites for water disinfection: current and future perspectives. *Environ. Pollut.* **298**, 118836. https://doi.org/10.1016/j.envpol.2022.118836 (2022).
41. Hafezieh, M., Kakoolaki, S., Ghasemi, M., Kazempoor, R. & Hemati, A. Blood and enzyme factors changes in New Zealand rabbit (Oryctolagus cuniculus) as an animal model in response to killed hemorrhagic septicemia virus (VHSv) virulent to Oncorhynchus mykiss. *Sustainable Aquaculture Health Manage. J.* **8**, 61–77. https://doi.org/10.52547/ijaah.8.1.61 (2022).
42. Sawai, J. Quantitative evaluation of antibacterial activities of metallic oxide powders (ZnO, MgO and CaO) by conductimetric assay. *J. Microbiol. Methods*. **54**, 177–182 (2003).
43. Moshafi, M. H., Ranjbar, M., Zeinalizadeh Rafsanjnai, Z. & Mehrabi, F. Preparation and evaluation of the Physicochemical and Antimicrobial properties of Biological nanostructures Polyolactic Acid/Calcium Oxide by Hydrothermal assisted microwave method. *Iran. J. Med. Microbiol.* **14**, 227–240 (2020).
44. Marquis, G., Ramasamy, B., Banwarilal, S. & Munusamy, A. P. Evaluation of antibacterial activity of plant mediated CaO nanoparticles using Cissus quadrangularis extract. *J. Photochem. Photobiol., B*. **155**, 28–33 (2016).
45. Alizadeh-Sani, M. et al. Kinetics analysis and susceptibility coefficient of the pathogenic bacteria by titanium dioxide and zinc oxide nanoparticles. *Adv. Pharm. Bull.* **10**, 56 (2020).
46. Ahmadi Shadmehri, A., Namvar, F., Miri, H. & Yaghmaei, P. Nakhaei Moghaddam, M. Assessment of antioxidant and antibacterial activities of Zinc Oxide nanoparticles, Graphene and Graphene decorated by Zinc Oxide nanoparticles. *Int. J. Nano Dimension*. **10**, 350–358 (2019).
48. Paunova-Krasteva, T. et al. Hybrid chitosan/CaO-based nanocomposites doped with plant extracts from Azadirachta indica and Melia azedarach: evaluation of antibacterial and antibiofilm activities. *Bionanoscience* **13**, 88–102 (2023).
49. Yusof, N. A. A., Zain, N. M. & Pauzi, N. Synthesis of ZnO nanoparticles with chitosan as stabilizing agent and their antibacterial properties against Gram-positive and Gram-negative bacteria. *Int. J. Biol. Macromol.* **124**, 1132–1136 (2019).
50. Sivakumar, P., Lee, M., Kim, Y. S. & Shim, M. S. Photo-triggered antibacterial and anticancer activities of zinc oxide nanoparticles. *J. Mater. Chem. B*. **6**, 4852–4871 (2018).
52. El-Liethy, M. A., Hemdan, B. A. & El-Taweel, G. E. Prevalence of E. Coli, Salmonella, and Listeria spp. as potential pathogens: a comparative study for biofilm of sink drain environment. *J. Food Saf.* **40**, e12816 (2020).
53. Hemdan, B. A., El-Liethy, M. A. & ElMahdy, M. & El-Taweel, G. E. Metagenomics analysis of bacterial structure communities within natural biofilm. *Heliyon* **5** (2019).
54. Vi, T. T. T. et al. Synergistic antibacterial activity of silver-loaded graphene oxide towards Staphylococcus aureus and Escherichia coli. *Nanomaterials* **10**, 366. https://doi.org/10.3390/nano10020366 (2020).
55. Aunkor, M. T. H. et al. Antibacterial activity of graphene oxide nanosheet against multidrug resistant superbugs isolated from infected patients. *Royal Soc. open. Sci.* **7**, 200640 (2020).
56. Hashemi, T., Habibi, N., Goli, H. & Hashemi, E. Synthesis of graphene nanoparticles and its antibacterial effects on *Staphylococcus aureus* and *Escherichia coli*. *J. Mol. Cell. Res.* **32**, 524–529 (2019). (In Farsi).
57. Hegyi, A. et al. Influence of TiO2 nanoparticles on the resistance of Cementitious Composite materials to the action of Bacteria. *Materials* **14**, 1074. https://doi.org/10.3390/ma14051074 (2021).
58. Silva, C. et al. Mechanical and antimicrobial polyethylene composites with CaO nanoparticles. *Polymers* **12**, 2132 (2020).
59. Parvathi, V. P., Umadevi, M. & Raj, R. B. Improved waste water treatment by bio-synthesized graphene sand composite. *J. Environ. Manage.* **162**, 299–305 (2015).
60. Olczak, K., Jakubowski, W. & Szymański, W. Bactericidal activity of Graphene Oxide tests for selected microorganisms. *Materials* **16**, 4199 (2023).
61. Akhavan, O. & Ghaderi, E. Toxicity of graphene and graphene oxide nanowalls against bacteria. *ACS nano*. **4**, 5731–5736. https://doi.org/10.1021/nn101390x (2010).
62. Bousiakou, L. G., Qindeel, R., Al-Dossary, O. M. & Kalkani, H. Synthesis and characterization of graphene oxide (GO) sheets for pathogen inhibition: Escherichia coli, Staphylococcus aureus and Pseudomonas aeruginosa. *J. King Saud University-Science*. **34**, 102002. https://doi.org/10.1016/j.jksus.2022.102002 (2022).
63. Mondal, T., Bhowmick, A. K. & Krishnamoorti, R. Chlorophenyl pendant decorated graphene sheet as a potential antimicrobial agent: synthesis and characterization. *J. Mater. Chem.* **22**, 22481–22487. https://doi.org/10.1039/c2jm33398h (2012).
64. Assali, M., Almasri, M., Kittana, N. & Alsouqi, D. Covalent functionalization of graphene sheets with different moieties and their effects on biological activities. *ACS Biomaterials Sci. Eng.* **6**, 112–121 (2019).
65. Kovtyukhova, N. I. et al. Layer-by-layer assembly of ultrathin composite films from micron-sized graphite oxide sheets and polycations. *Chem. Mater.* **11**, 771–778 (1999).
66. Chowdhuri, A. R., Tripathy, S., Chandra, S., Roy, S. & Sahu, S. K. A ZnO decorated chitosan–graphene oxide nanocomposite shows significantly enhanced antimicrobial activity with ROS generation. *RSC Adv.* **5**, 49420–49428. https://doi.org/10.1039/C5RA05393E (2015).
67. Wanag, A. et al. Antibacterial properties of TiO2 modified with reduced graphene oxide. *Ecotoxicol. Environ. Saf.* **147**, 788–793 (2018).
68. Bwatanglang, I. B., Magili, S. T. & Kaigamma, I. Adsorption of phenol over bio-based silica/calcium carbonate (CS-SiO2/CaCO3) nanocomposite synthesized from waste eggshells and rice husks. *PeerJ Phys. Chem.* **3**, e17 (2021).
69. Le, T. L. T. et al. Controlled growth of TiO2 nanoparticles on graphene by hydrothermal method for visible-light photocatalysis. *J. Science: Adv. Mater. Devices*. **6**, 516–527. https://doi.org/10.1016/j.jsamd.2021.07.003 (2021).
70. Wang, J., Wei, Y., Shi, X. & Gao, H. Cellular entry of graphene nanosheets: the role of thickness, oxidation and surface adsorption. *RSC Adv.* **3**, 15776–15782 (2013).
71. Khan, S. A. et al. Synthesis of TiO2/Graphene oxide nanocomposites for their enhanced photocatalytic activity against methylene blue dye and ciprofloxacin. *Compos. Part. B: Eng.* **175**, 107120 (2019).
72. Khine, E. E. et al. Synthesis and characterization of calcium oxide nanoparticles for CO2 capture. *J. Nanopart. Res.* **24**, 139 (2022).
73. Wang, M. et al. Preparation of high-surface-area carbon nanoparticle/graphene composites. *Carbon* **50**, 3845–3853 (2012).
74. Er, S. G., Edirisinghe, M. & Tabish, T. A. Graphene-Based Nanocomposites as Antibacterial, Antiviral and Antifungal agents. *Adv. Healthc. Mater.* **12** (2023).
75. Song, J., Zhang, J., Zheng, K., Xu, Z. & Qi, K. Development process of graphene field for photocatalytic and antibacterial applications. *Desalination Water Treat.* **297**, 117–130 (2023).
76. Ghasemi, S., Esfandiar, A., Setayesh, S. R., Habibi-Yangjeh, A. & Gholami, M. Synthesis and characterization of TiO2–graphene nanocomposites modified with noble metals as a photocatalyst for degradation of pollutants. *Appl. Catal. A*. **462**, 82–90 (2013).
77. Kusiak-Nejman, E. & Morawski, A. W. TiO2/graphene-based nanocomposites for water treatment: a brief overview of charge carrier transfer, antimicrobial and photocatalytic performance. *Appl. Catal. B*. **253**, 179–186 (2019).
78. Hajduga, M. B. et al. The influence of Graphene Content on the Antibacterial properties of Polycaprolactone. *Int. J. Mol. Sci.* **23**, 10899 (2022).
79. Bykkam, S. et al. Few layered graphene sheet decorated by ZnO nanoparticles for anti-bacterial application. *Superlattices Microstruct.* **83**, 776–784. https://doi.org/10.1016/j.spmi.2015.03.063 (2015).
80. Zinadini, S. et al. Preparation and characterization of antifouling graphene oxide/polyethersulfone ultrafiltration membrane: application in MBR for dairy wastewater treatment. *J. Water Process. Eng.* **7**, 280–294. https://doi.org/10.1016/j.jwpe.2015.07.005 (2015).

81. Jiang, Q., Liu, J., Qi, T. & Liu, Y. Enhanced visible-light photocatalytic activity and antibacterial behaviour on fluorine and graphene synergistically modified TiO(2) nanocomposite for wastewater treatment. *Environ. Technol.* 1–14. https://doi.org/10.1080/09593330.2021.1936198 (2021).
82. Rathnayake, D., Krishna, K. B., Kastl, G. & Sathasivan, A. The role of pH on sewer corrosion processes and control methods: a review. *Sci. Total Environ.* **782**, 146616 (2021).

Author contributions
R.D and H.A wrote the main manuscript text and H.B prepared figures. All authors reviewed the manuscript.

Declarations

Competing interests
The authors declare no competing interests.

Additional information
Correspondence and requests for materials should be addressed to H.A.

Reprints and permissions information is available at www.nature.com/reprints.

Publisher's note Springer Nature remains neutral with regard to jurisdictional claims in published maps and institutional affiliations.